

Article

Impediment of Iron Corrosion by *N,N'*-Bis[2-hydroxynaphthylidene]amino]oxamide in 3.5% NaCl Solution

El-Sayed M. Sherif ^{1,*} , Ayman H. Ahmed ^{2,3} , Hany S. Abdo ¹  and Monerah N. DefAllah ⁴

¹ Center of Excellence for Research in Engineering Materials (CEREM), College of Engineering, King Saud University, P.O. Box 800, Al-Riyadh 11421, Saudi Arabia; habdo@ksu.edu.sa

² Chemistry Department, College of Science and Arts, Jouf University, Gurayat 2014, Saudi Arabia; ahfahmi@ju.edu.sa

³ Department of Chemistry, Faculty of Science, Al-Azhar University, Nasr City 11884, Egypt

⁴ Department of Chemistry, Faculty of Science, Taif University, Hawiya 888, Saudi Arabia; monerahn2021@gmail.com

* Correspondence: esherif@ksu.edu.sa

Abstract: Hydrazone [*N,N'*-bis[2-hydroxynaphthylidene]amino]oxamide] derived from the condensation of ethanedihydrazide with 2-hydroxynaphthalene-1-carbaldehyde was synthesized and assessed on the basis of elemental analysis (CHN) and spectral (IR, mass, ¹³C/¹H NMR and UV-Vis) measurements. The influence of *N,N'*-bis[2-hydroxynaphthylidene]amino]oxamide (HAO) in terms of the inhibition of iron corrosion in concentrated sodium chloride solution (3.5 wt.% NaCl) after various exposure periods was assessed. Numerous electrochemical and spectroscopic assessment techniques were performed. Cyclic potentiodynamic polarization experiments indicated that the presence of HAO and its increased concentration decreased the corrosion of iron in NaCl solution by decreasing the corrosion values, anodic and cathodic currents, and corrosion rate. The electrochemical impedance spectroscopy results showed that HAO molecules greatly increased the corrosion resistance. The chronoamperometric experiments performed at −475 mV (Ag/AgCl) revealed that the HAO molecules decreased the absolute currents and reduced the probability of the occurrence of pitting corrosion. The effect of HAO on the inhibition of iron corrosion was also confirmed through scanning electron microscopy micrographs and energy-dispersive X-ray profile analyses, which proved that the surface of the iron sample exposed to chloride solution alone was pitted, while the presence of HAO molecules reduced the severity of the pitting corrosion. The results confirmed that the presence of HAO molecules inhibits the corrosion of iron and this impact increased when the exposure time was increased to 48 h.

Keywords: oxamides; iron corrosion; organic inhibitors; cyclic polarization; electrochemical impedance spectroscopy



Citation: Sherif, E.-S.M.; Ahmed, A.H.; Abdo, H.S.; DefAllah, M.N. Impediment of Iron Corrosion by *N,N'*-Bis[2-hydroxynaphthylidene]amino]oxamide in 3.5% NaCl Solution. *Crystals* **2021**, *11*, 1263. <https://doi.org/10.3390/cryst11101263>

Academic Editors: Vladislav V. Kharton, Changhong Wang and Xiaofei Yang

Received: 20 September 2021

Accepted: 15 October 2021

Published: 18 October 2021

Publisher's Note: MDPI stays neutral with regard to jurisdictional claims in published maps and institutional affiliations.



Copyright: © 2021 by the authors. Licensee MDPI, Basel, Switzerland. This article is an open access article distributed under the terms and conditions of the Creative Commons Attribution (CC BY) license (<https://creativecommons.org/licenses/by/4.0/>).

1. Introduction

N,N'-bis[2-hydroxynaphthylidene]amino]oxamide is an example of polyfunctional hydrazones, which are organic compounds that have fascinating biological properties, such as anti-inflammatory, analgesic, anticonvulsant, antitumor, and anti-HIV properties [1]. Additionally, they are significant in drug design and organocatalysis and have uses as inhibitors and antioxidants [2]. In analytical chemistry, some hydrazones have been employed as indicators [3] and analytical reagents for the extraction of copper(II), nickel(II), and cobalt(II) traces [4–6].

Previous studies have reported that numerous organic compounds have been utilized as inhibitors in controlling the corrosion of iron in 3.5% NaCl [7–12]. Macedo et al. [7] studied the inhibition mechanism of imidazole and some of their derivatives onto the surface of an iron sample in 3.5% NaCl medium. The outcomes showed that the considered

compounds act with anodic corrosion inhibitors for iron in saline medium. Aslam et al. investigated the inhibitory behavior of *N,N'*-didodecyl-*N,N'*-digluconamideethylenediamine gemini surfactant on mild steel (MS) corrosion in 3.5% NaCl at 30–60 °C [8]. The compound mitigated the corrosion and the degree of inhibition was dependent on the concentration and temperature. Moreover, 1,1'-thiocarbonyldiimidazole [9], 5-(3-aminophenyl)-tetrazole [10], sodium 2-(4-(benzo[d]thiazol-2-ylthio)-6-(hexylamino)-1,3,5-triazin-2-ylamino)ethanesulfonate [11], (3-amino-1,2,4-triazole-5-thiol and 1,1'-thiocarbonyldiimidazole) [12], (2-sulfhydryl)-(5-phenmethyl)-(1-(4-phenol)-methanimine)-triazole [13], 1-butyl-3-methylimidazolium chloride [14], polyethyleneimine [15], and cetylpyridinium chloride [16] have been tested as inhibitors for different species of iron in the same medium. With respect to hydrazones, some compounds have been examined as inhibitors in various media for different metals, especially for iron species, which have shown potential inhibition efficiency [17–24]. *N,N'*-bis[2-hydroxynaphthylidene]amino]oxamide, which is regarded as one of the hydrazone compounds, was employed as a corrosion inhibitor towards the aluminum, copper, and carbon-steel in 1M HCl solutions using traditional weight loss measurements [25–27].

A literature survey revealed that the impediment of iron corrosion by *N,N'*-bis[2-hydroxynaphthylidene]amino]oxamide in a near-neutral concentrated chloride solution had not yet been achieved. Actually, the organic compounds containing heteroatoms such as nitrogen, oxygen, phosphor, and sulfur, as well as multiple bonds in their molecular structures, are mostly proficient inhibitors of metallic corrosion (M = copper, iron, aluminum, etc.) in NaCl brine and other media through eliminating the undesirable destructive influence of the corrosive media towards the metal surface [28–32]. The action of these inhibitors is clearly attributed to the physical or chemical adsorption of their molecules onto the surface of the metal [33–36]. In addition, the molecular weights and structures of the organic molecules are important parameters to be considered when choosing an organic corrosion inhibitor [37–39]. The aromatic *N,N'*-bis[2-hydroxynaphthylidene]amino]oxamide was speculated to have excellent inhibition efficiency for iron due to its adequate molecular structure that contains adsorption centers (N, O) and π -bonds, which enable it to bind strongly with the iron sample's surface.

In view of the inhibitive impacts of organic compounds containing N and O heteroatoms, we were motivated to investigate the influence of small concentrations of a synthesized aromatic hydrazone named *N,N'*-bis[2-hydroxynaphthylidene]amino]oxamide (HAO) on the corrosion of pure iron in freely aerated 3.5% NaCl solutions after exposure periods of 1 and 48 h. The study was achieved through various electrochemical techniques, namely cyclic potentiodynamic polarization, chronoamperometric current–time at fixed value of potential (−475 mV (Ag/AgCl)), and electrochemical impedance spectroscopy, after the iron was immersed in the different solutions for 1 and 48 h before measurement. The scanning electron microscopy and energy-dispersive X-ray analyses were employed to investigate the morphology and compositions of the surfaces after being exposed to the chloride solution without and with HAO molecules present. It is suggested that the presence of HAO molecules would hinder the corrosion of iron via their adsorption onto the external surface, which would diminish the corrosion rate and increment of the corrosion resistance.

2. Experimental

2.1. Materials and Methods

Ethanedihydrazide (EH) and 2-hydroxynaphthalene-1-carbaldehyde were purchased from Sigma-Aldrich (Gillingham, Dorset, UK). HAO powder was dissolved in dimethylformamide (DMF) to prepare a stock solution of 0.01 M. The desired chloride solutions with or without the existence of the tested HAO were synthesized from the stock solutions by dilution. Sodium chloride (99% purity) was purchased from Merck. Other chemicals and solvents were of the highest purity and used without further purification. The elemental analysis (CHN), mass spectrum analysis using the direct inlet system, and FT-IR were

carried out as reported [40]. ^{13}C -NMR (at 75.46 MHz) and ^1H -NMR (at 300 MHz) measurements in dimethylsulphoxide (DMSO- d_6) at room temperature (RT) were performed using a Varian mercury VX-300 NMR spectrometer. The chemical shifts are quoted in δ (ppm) with the aid of an internal reference (tetramethylsilane, TMS). The UV-visible absorptions were scanned on a Shimadzu (UV-1900) spectrophotometer between 200 and 1100 nm. A scanning electron microscope (SEM) with an attached unit for an energy-dispersive X-ray (EDX) analyzer was used to obtain the SEM micrographs and the EDX profiles. The SEM/EDX machine was a JEOL JSM-7400F microscope (Tokyo, Japan). The secondary electron and back-scattered electron detector was an Everhart–Thornley instrument working in automatic mode. The microscopy machine was operated at 15 kV.

The electrochemical measurements were performed in a traditional three-electrode electrochemical cell that accommodated 250 mL solution. The working electrode was a pure iron electrode (99.999% purity) with a surface area of 0.25 cm^2 . This iron rod was purchased from Goodfellow (located at Ermine Business Park, Huntingdon, UK) and used as the working electrode in this examination. A Pt sheet and silver–silver chloride (Ag/AgCl in saturated KCl solution) were the counter and reference electrodes, respectively. Electrochemical experiments were performed using a PGSTAT-302N Autolab Potentiostat. CPP curves were measured between -1200 and $+100$ mV at a scan rate of 0.00166 V/s. The PCT was measured at a value of -475 mV vs. Ag/AgCl for 1 h. EIS plots were obtained from the open-circuit potential values at a frequency scan range of 100,000 to 0.1 Hz with ± 5 mV amplitude sinusoidal wave perturbation.

2.2. Isolation of *N,N*-bis([2-hydroxynaphthylidene]amino)oxamide

N,N'-bis[2-hydroxynaphthylidene]amino]oxamide (HAO) was prepared using the same recipe published earlier [41–43]. By heating on a hot plate, ethanedihydrazide (0.02 mol) was allowed to dissolve in 80 mL distilled water, then 30 mL absolute ethanol was added. The subsequent hot ethanedihydrazide solution was mixed well with a hot ethanolic solution of 2-hydroxynaphthalene-1-carbaldehyde (0.04 mol). During the gradual addition of aldehyde, sedimentation of oxamide was noticed. The resulting mixture was refluxed for 3 h with constant stirring. The desired oxamide was collected by concentrating the solution to half of its volume and cooling. Next, the product was isolated by filtration and then washed vigorously with hot water and absolute ethanol. Finally, the solid compound was dried at 80 $^\circ\text{C}$ for 3 h inside an electric oven. The molecular formula of the HAO was assured by elemental analysis, which was conducted as follows: HAO oxamide/ $\text{C}_{24}\text{H}_{18}\text{N}_4\text{O}_4$ (Mol. Wt. = 426.13), 67.60% C, 4.25% H, 13.14% N. The % values of the elements were also experimentally obtained as follows: 68.30% C, 5.11% H, 12.84% N. Furthermore, the structural formula of oxamide was determined based on IR, $^1\text{H}/^{13}\text{C}$ NMR, and mass spectroscopy data, as will be shown later in this paper.

3. Results and Discussion

3.1. Chemistry and Characterization of the Inhibitor (HAO)

The *N,N'*-bis[2-hydroxynaphthylidene]amino]oxamide inhibitor was isolated in a pure form. The physical properties of the compound and its corresponding hydrazide are shown in Table 1. The template synthesis of HAO derived from ethanedihydrazide and aldehyde is represented in Scheme 1. The chosen oxamide (HAO) was dissolved in DMF to prepare a stock solution. The low concentrations of HAO of 5×10^{-5} , 10^{-4} , and 5×10^{-4} M were prepared by dilution and added to 3.5% NaCl solution to obtain the desired electrolyte.

Table 1. Physical data of the inhibitor (HAO) and its corresponding hydrazide (EH).

Compound (Formula/Symbol)	Color	Melting Point	Yield %
Ethanedihydrazide ($\text{C}_2\text{H}_6\text{N}_4\text{O}_2$ /EH)	White	242–244 $^\circ\text{C}$	*
<i>N,N'</i> -bis[2-hydroxynaphthylidene]amino]oxamide ($\text{C}_{24}\text{H}_{18}\text{N}_4\text{O}_4$ /HAO)	Yellow	>300 $^\circ\text{C}$	98

* Purchased from Sigma-Aldrich.

Indeed, the presented work is considered an extension of prior studies. The configuration of the chosen inhibitor was discussed in detail elsewhere [25–27,41]. The structural formula of the synthesized HAO inhibitor was validated on this basis.

3.1.1. IR Spectra

The IR spectra of HAO and its corresponding EH are displayed in Figure 1, showing the EH has νNH (3200 cm^{-1}), $\nu\text{C=O}$ (1680 cm^{-1}), δNH_2 (1307 cm^{-1}) and amide $\delta\text{O=C-N}$ (792 cm^{-1}). The very strong bands at 3300 and 3265 cm^{-1} are most probably due to asymmetric and symmetric NH_2 stretching vibrations, respectively. HAO uncovered bands for νNH (3166 cm^{-1}), $\nu\text{OH}_{\text{naphthoic}}$ (3476 cm^{-1}), $\nu\text{C=O}$ ($1705\text{ cm}^{-1} + 1660\text{ cm}^{-1}$), $\nu\text{C-O}_{\text{naphthoic}}$ (1287 cm^{-1}), and $\nu\text{C=N}$ (1621 cm^{-1}). Obscure bands of νNH_2 accompanying the appearance of $\nu\text{C=N}$ in the spectra of HAO demonstrate the successful condensation between EH and the utilized aldehyde.

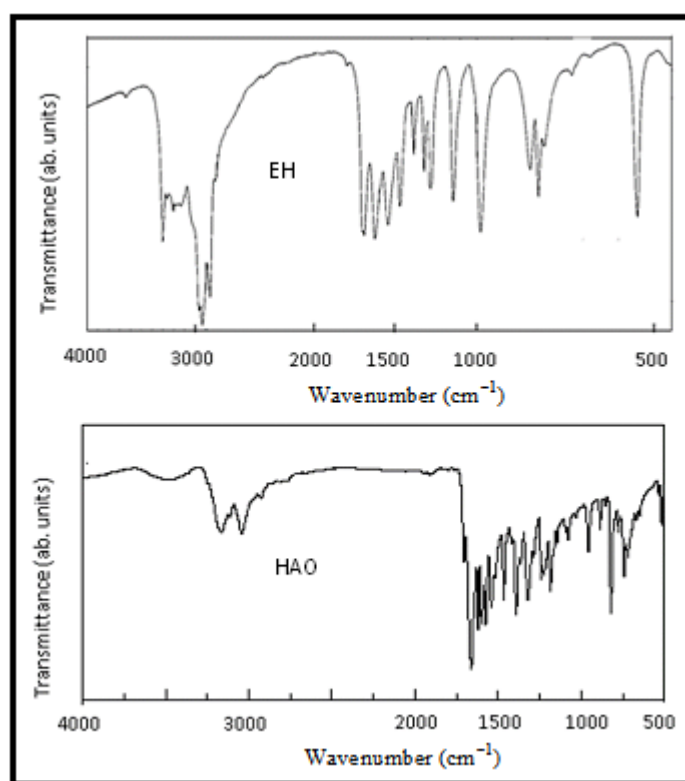


Figure 1. FT-IR spectra of EH and HAO, respectively.

3.1.2. Mass Spectra

The mass spectra of HAO (Figure 2) affirmed its correct molecular weight, exhibiting a molecular ion peak at: $m/z = 427$ (20%, $\text{C}_{16}\text{H}_{14}\text{N}_4\text{O}_4$), calculated $m/z = 426.4$). Other ion peaks were exhibited at $m/z = 50$ [100%, base peak, $\text{M}^+(\text{C}_4\text{H}_4)$], 64.95 [71%, $\text{M}^+(\text{C}_5\text{H}_5)$], 79 [40%, $\text{M}^+(\text{C}_6\text{H}_8)$], 128 [37%, $\text{M}^+(\text{C}_{10}\text{H}_8)$], 141 [4%, $\text{M}^+(\text{C}_{11}\text{H}_9)$], 175 [71%, $\text{M}^+(\text{C}_{11}\text{H}_9\text{NO})$], 242 [40%, $\text{M}^+(\text{C}_{13}\text{H}_9\text{N}_2\text{O}_3)$], 257 [50%, $\text{M}^+(\text{C}_{13}\text{H}_{10}\text{N}_3\text{O}_3)$], 157 [21.2%, $\text{M}^+(\text{C}_{11}\text{H}_9\text{O})$], and 270 [21%, $\text{M}^+(\text{C}_{13}\text{H}_{10}\text{N}_4\text{O}_3)$], in addition to 410 [25%, $\text{M}^+(\text{C}_{24}\text{H}_{18}\text{N}_4\text{O}_3)$].

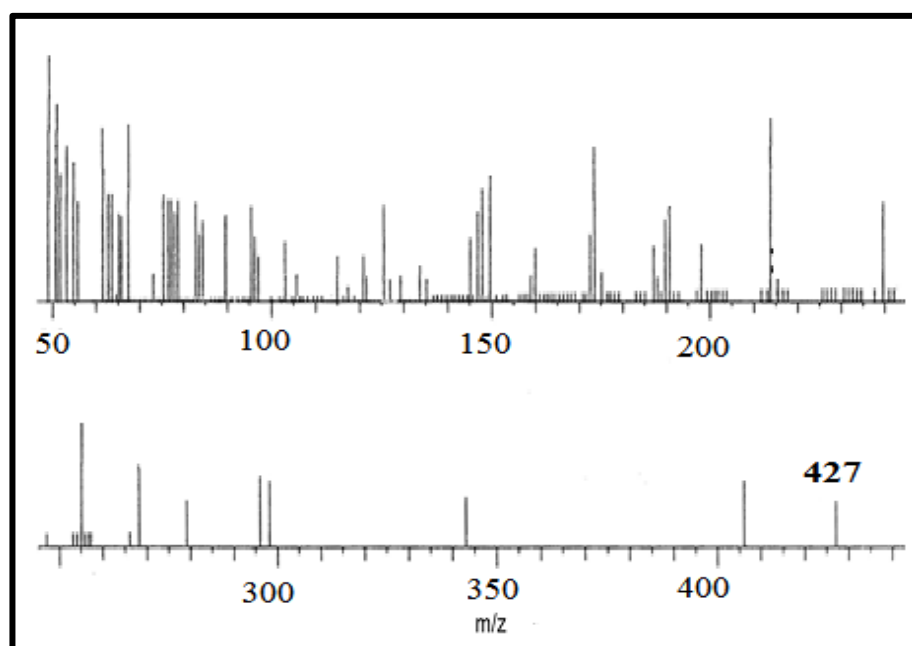


Figure 2. Mass spectrum of HAO.

3.1.3. ^{13}C NMR Spectra

^{13}C NMR: The spectrum of HAO is depicted in Figure 3. HAO showed resonances at 155.7 ppm for C=O; 149.7 ppm for C=N; and 158.3, 132.5, 128.9, 127.8, and 123.6 for Ar-C2, Ar-C4, Ar-C6, Ar-C5, and Ar-C1, respectively. It is suggested that the obtained spectral lines represent more carbon types in the represented structure due to the presence of some molecules in dienol or diketo forms.

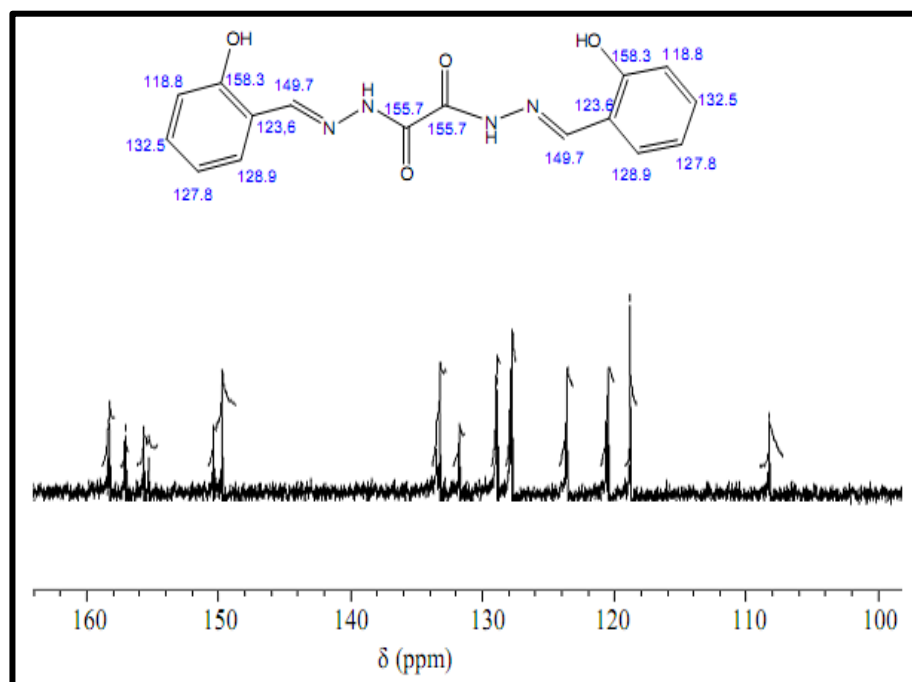


Figure 3. ^{13}C NMR spectrum of HAO in $\text{DMSO-}d_6$ at RT.

3.1.4. ^1H NMR Spectra

In Figure 4, HAO revealed signals at: 9.7 (CH=N, s), 12.8 (NH, s), 12.6 (naphthoic OH, s), and 7.0–8.8 (aromatic protons, m). Vanishing signals of –OH and –NH upon D_2O

addition indicated the right positions of these groups. Because deuterium is invisible in the ^1H NMR spectrum and the proton in $-\text{OH}$ and $-\text{NH}-$ groups is labile (acidic proton), doping the NMR sample with D_2O easily exchanged out these protons for deuterium, resulting in the disappearance of labile proton peaks.

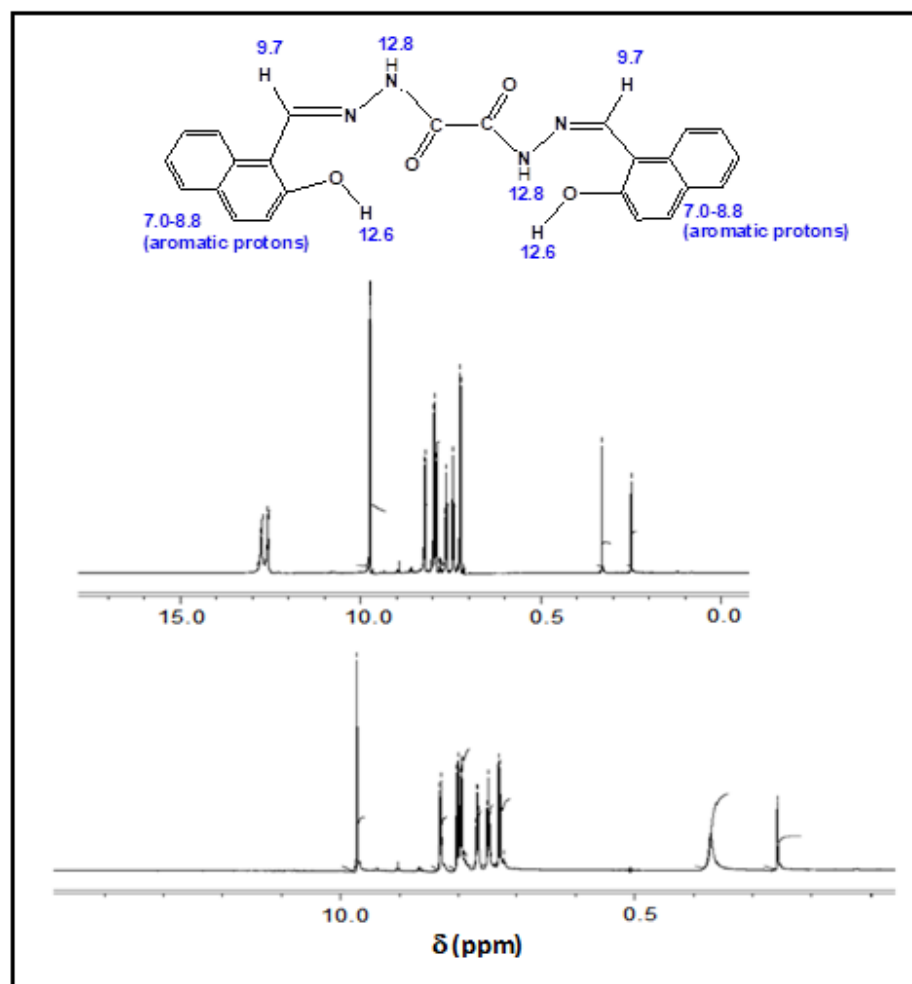


Figure 4. ^1H NMR spectrum of HAO in $\text{DMSO}-d_6$ at RT.

3.1.5. Electronic Spectra

The UV-visible spectra of the EH and its HAO derivative were scanned in DMF and are shown in Figure 5. The electronic data for the studied compounds exhibited one absorption band for EH and five absorption bands for the HAO inhibitor as follows: EH: λ_{max} (nm) equals 375 ($n-\pi^*$, $\text{C}=\text{O}$) and 271 ($\pi-\pi^*$, $\text{C}=\text{O}$); HO: λ_{max} (nm) equals 330 ($n-\pi^*$, $\text{C}=\text{N}$), 328 ($n-\pi^*$, $\text{C}=\text{O}$), 314 ($\pi-\pi^*$, $\text{C}=\text{N}$), 300 ($\pi-\pi^*$, $\text{C}=\text{O}$), and 270 ($\pi-\pi^*$, aromatic ring).

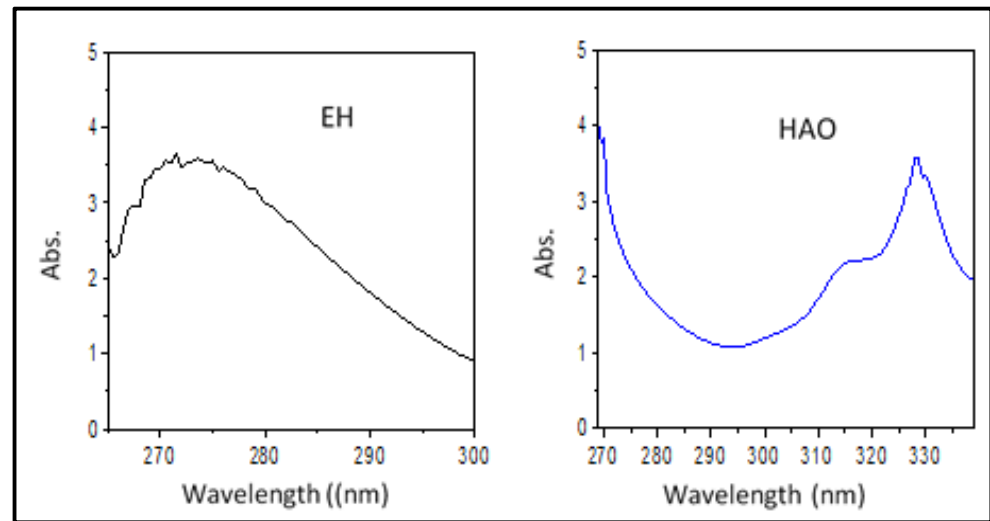


Figure 5. UV-visible spectra of EH and its HAO derivative in DMF.

3.2. Corrosion Measurements

3.2.1. Cyclic Polarization Data

The cyclic potentiodynamic polarization (CPP) measurements were carried out to report the corrosion parameters and to evaluate the corrosion and corrosion inhibition of iron in chloride solutions with and without HAO molecules present. CPP curves collected for iron electrodes in 3.5% NaCl solutions (a) without HAO and with (b) 5×10^{-5} M HAO, (c) 1×10^{-4} M HAO, and (d) 5×10^{-4} M HAO present after 1 h immersion in the different solutions before measurement are depicted in Figure 6. The CPP experiments were also obtained under the same conditions after prolonging the time of immersion in all solutions to 48 h, the curves for which are shown in Figure 7. The corrosion current (j_{Corr}), cathodic Tafel (β_c) slope, anodic Tafel (β_a) slope, corrosion potential (open-circuit potential, E_{Corr}), polarization resistance (R_p), and corrosion rate (K_{Corr}), in addition to the percentage of the inhibition efficiency (IE%) that were obtained from the polarization curves, are shown in Table 2.

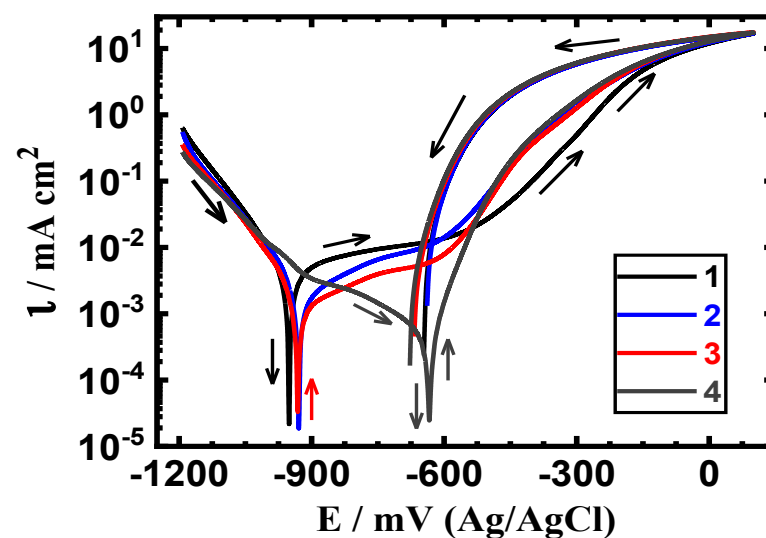


Figure 6. CPP curves for iron after 1 h immersion in (1) 3.5% NaCl solutions in the absence and presence of (2) 5×10^{-5} M HAO, (3) 1×10^{-4} M HAO, and (4) 5×10^{-4} M HAO.

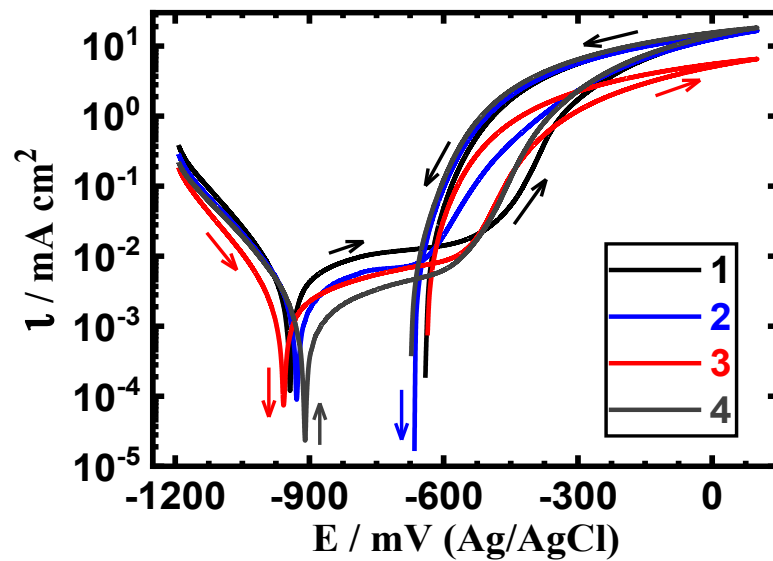


Figure 7. CPP curves for iron after 48 h immersion in (1) 3.5% NaCl solutions in the absence and presence of (2) 5×10^{-5} M HAO, (3) 1×10^{-4} M HAO, and (4) 5×10^{-4} M HAO.

Table 2. The data obtained from the polarization curves.

Solutions	$\beta_c/\text{mV dec}^{-1}$	$E_{\text{Corr}}/\text{mV}$	$\beta_a/\text{mV dec}^{-1}$	$j_{\text{Corr}}/\mu\text{A cm}^{-2}$	$R_p/\Omega \text{ cm}^2$	$K_{\text{Corr}}/\text{mmpy}$	IE/%
3.5% NaCl + 0.0 M HAO (1 h)	80	−945	115	3.2	641.03	0.0823	—
3.5% NaCl + 5×10^{-5} M HAO (1 h)	75	−925	98	1.5	1231.5	0.0174	53.13
3.5% NaCl + 1×10^{-4} M HAO (1 h)	70	−915	90	0.70	2445.7	0.0081	78.13
3.5% NaCl + 5×10^{-4} M HAO (1 h)	80	−655	75	0.50	3366.1	0.0058	84.36
3.5% NaCl + 0.0 M HAO (48 h)	70	−940	110	2.1	885.7	0.0540	—
3.5% NaCl + 5×10^{-5} M HAO (48 h)	75	−925	105	1.2	1585.1	0.0139	62.50
3.5% NaCl + 1×10^{-4} M HAO (48 h)	73	−945	95	0.65	2761.2	0.0076	79.69
3.5% NaCl + 5×10^{-4} M HAO (48 h)	68	−900	90	0.40	4210.3	0.0047	87.50

The values of E_{Corr} and j_{Corr} were obtained from the extrapolation of the cathodic and anodic Tafel lines that located next to the linearized current regions [44–49]. The values of R_p and K_{Corr} were calculated from the following equations, respectively [50,51];

$$R_p = \frac{1}{i_{\text{Corr}}} \left(\frac{\beta_c \cdot \beta_a}{2.3(\beta_c + \beta_a)} \right) \quad (1)$$

$$K_{\text{Corr}} = i_{\text{Corr}} \left(\frac{kE_W}{dA} \right) \quad (2)$$

The percentage of inhibition efficiency (IE%) was also obtained as follows [4,38];

$$\text{IE}\% = \frac{i_{\text{Corr}}^i - i_{\text{Corr}}^0}{i_{\text{Corr}}^0} \times 100 \quad (3)$$

where k equals 3272 and is the constant that defines the unit for the rate of corrosion (mm/amp cm year), E_W is the equivalent weight, d is the density, and A is the surface area. Additionally, i_{Corr}^0 and i_{Corr}^i are the corrosion current densities for iron in the absence and presence of the HAO, respectively.

The CPP curve obtained for iron in NaCl solution without HAO added (Figure 6, curve 1) showed a decrease in the cathodic current with a potential swept in the cathodic

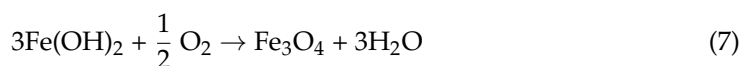
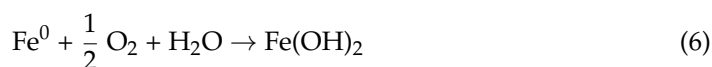
branch due to the reduction reaction that took place on the surface of the iron sample. This reaction was the reduction of oxygen on the surface of iron, as follows [10,44,52];



The minimum current was recorded at the value of j_{Corr} (the intersection of the extrapolation of the cathodic and anodic Tafel lines). The current then started to rise again in the anodic branch due to the dissolution of the iron sample as per the following equation [10,52];



The current then slightly slowed down, showing a passive region as a result of the reaction of the iron sample with oxygen from the solution to form iron hydroxide ($\text{Fe}(\text{OH})_2$) and iron oxide (Fe_3O_4), as follows [38];



The continuous sweeping of the potential in the positive direction in the presence of the chloride ions led to the breakdown of the formed oxide film, which was indicated by the abrupt increase in the current in the forward anodic side. Reversing the scanning the potential in the backward direction seemed to result in a higher current as compared to the obtained current in the forward direction. This led to the appearance of a hysteresis loop; the wide size of the hysteresis loop indicates the occurrence of pitting corrosion with high severity.

The addition of 5×10^{-5} M HAO to the chloride solution after 1 h immersion (Figure 6, curve 2) showed smaller cathodic and anodic currents as well as the smaller size of the hysteresis loop as compared to the one obtained for iron in chloride solution alone (Figure 6, curve 1). The data were obtained from Table 1, where the j_{Corr} and K_{Corr} showed smaller values as well. This confirms that the addition of 5×10^{-5} M HAO decreases the uniform and pitting corrosion. Increasing the concentration of HAO to 1×10^{-4} M led to introducing lower values of j_{Corr} and K_{Corr} , and this effect was further enhanced when the concentration of HAO was increased to 5×10^{-4} M. Perhaps this was due to the adsorption of HAO molecules onto the surface of the iron, leading to blocking of the flawed and pitted areas on the surface and suppressing its corrosion.

The CPP curves obtained after 48 h (Figure 7) showed similar behavior but with currents lower than those obtained for the iron after 1 h exposure in all solutions. The data listed in Table 1 confirm that the values of j_{Corr} and K_{Corr} decreased for iron after 48 h immersion in all solutions as compared to the values obtained after only 1 h immersion, regardless of whether HAO molecules were present or not. For j_{Corr} , a value of $3.2 \mu\text{A}/\text{cm}^2$ was recorded for iron in chloride solution alone after 1 h immersion, which increased to $2.1 \mu\text{A}/\text{cm}^2$ for iron in chloride solution alone after 48 h exposure. These values decreased in the presence of 5×10^{-5} M HAO to $1.5 \mu\text{A}/\text{cm}^2$ and $1.2 \mu\text{A}/\text{cm}^2$. It is also worth mentioning that lower values were recorded for iron in chloride solution in the presence of 5×10^{-4} M HAO after 1 and 48 h, with values of $0.5 \mu\text{A}/\text{cm}^2$ and $0.4 \mu\text{A}/\text{cm}^2$, respectively. The values of K_{Corr} also decreased and R_p values increased in the same order as those obtained for j_{Corr} . This proved that the presence and increase of HAO molecules decrease the corrosion of iron and that this effect increases with prolonged exposure time from 1 to 48 h.

3.2.2. Chronoamperometric Current–time Results

In order to shed more light on the effect of HAO on the inhibition of iron corrosion and the possibility of the occurrence of pitting corrosion in the chloride solution at a constant potential, chronoamperometric current–time measurements were carried out. The

chronoamperometric current with time measurements for iron in (1) 0.0 HAO, (2) 5×10^{-5} HAO, (3) 1×10^{-4} HAO, and (4) 5×10^{-4} M HAO obtained at -475 mV (Ag/AgCl) were performed after 1 and 48 h immersion, the curves of which are shown in Figures 8 and 9, respectively. It can be seen from Figure 3 that the currents for iron in all solutions showed very low values, possibly due to the formation of an oxide film during the immersion of iron for 1 h before applying the anodic potential. The recorded current increased with increasing time of the experiment as a result of the dissolution of the oxide film and the continued increments in current due to the occurrence of pitting corrosion.

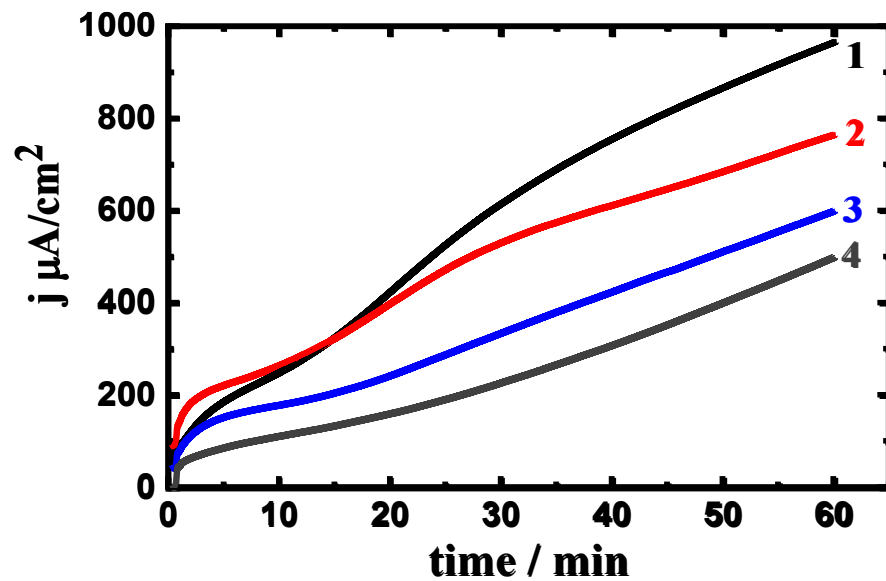


Figure 8. Current curves collected at -475 mV (Ag/AgCl) for iron in 3.5% NaCl solutions containing (1) 0.0, (2) 5×10^{-5} , (3) 1×10^{-4} , and (4) 5×10^{-4} M HAO after 1 h immersion.

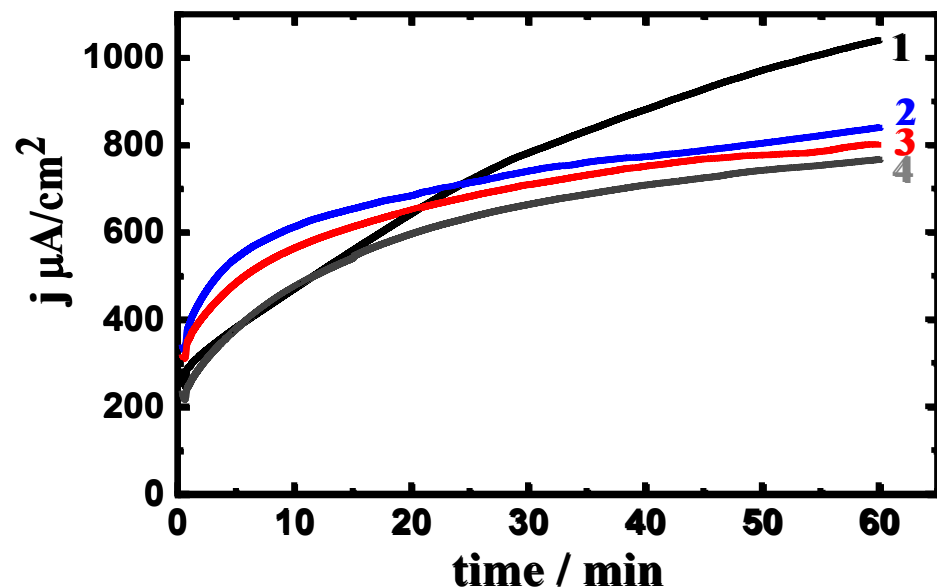


Figure 9. Current curves collected at -475 mV (Ag/AgCl) for iron in 3.5% NaCl solutions containing (1) 0.0, (2) 5×10^{-5} , (3) 1×10^{-4} , and (4) 5×10^{-4} M HAO after 48 h immersion.

The presence of 5×10^{-5} M HAO, as shown in Figure 8 (curve 2), resulted in almost the same current–time behavior but with lower absolute values for the recorded current. This decrease in the current values indicated that 5×10^{-5} M HAO inhibits the dissolution of iron via reducing the uniform and pitting corrosion. Increasing the content of HAO to

1×10^{-4} M, as shown in Figure 8 (curve 3), greatly decreased the obtained current values through the whole time of the experiment as compared to the current values collected for NaCl alone and NaCl + 5×10^{-5} M HAO, confirming that the increase of HAO from 5×10^{-5} M to 1×10^{-4} M greatly reduced both the uniform and pitting corrosion for iron. This suggestion was further supported by the increase of HAO molecules to 5×10^{-4} M, as shown in Figure 3 (curve 4), as the obtained current at this concentration was the lowest.

Figure 9 shows the current–time curves for iron samples that were immersed in the chloride solutions in the absence and presence of HAO molecules for 48 h before fixing the constant potential for 1 h. It can be seen that the increase in the current with time continued and was the highest for iron in NaCl solution that had no HAO present, proving that NaCl solution had harsh effects on the surface. The presence of 5×10^{-5} M HAO (Figure 9, curve 2) decreased the overall currents, and this effect increased with the increases of the HAO content to 1×10^{-4} M and 5×10^{-4} M. Extending the exposure time of iron in the different solutions reduced the corrosiveness of the chloride ions by decreasing the current obtained over time, particularly when HAO molecules were present. The change of current with time measurements confirmed the results of the CPP measurements.

3.2.3. EIS Data

In order to confirm the data obtained from the CPP and current–time experiment, EIS measurements were carried out. It has been reported [53–58] that the EIS method can be successfully employed to understand corrosion and corrosion protection for metals and alloys in the surrounding environments. Figure 10 presents the collected Nyquist plots for the iron samples that were immersed for 1 h in 3.5% NaCl solutions without (a) and with (b) 5×10^{-5} M HAO, (c) 1×10^{-4} M HAO, and (d) 5×10^{-4} M HAO. The Nyquist plots were also obtained after 48 h immersion in the different solutions, as shown in Figure 11. All impedance data were best fitted to the equivalent circuit model that is depicted in Figure 12. The values of the impedance parameters of the circuit were obtained and are listed in Table 3. These parameters were R_s (solution resistance), Q (constant phase elements, CPEs), and R_p (polarization resistance). The values of the inhibition efficiency (IE/%), which were obtained for the HAO inhibitor, are also presented in Table 3 and were obtained as per the following relation [56–58];

$$IE\% = \frac{R_p^{In} - R_p^{Un}}{R_p^{Un}} \times 100 \quad (8)$$

Table 3. EIS parameters obtained by fitting the impedance data for iron in chloride solutions with and without HAO molecules.

Parameter/Solution	$R_s/\Omega \text{ cm}^2$	Q (CPEs)		$R_p/\Omega \text{ cm}^2$	IE/%
		$Y_Q/\mu\text{F cm}^{-2}$	n		
3.5% NaCl + 0.0 M HAO (1 h)	9.40	7.14	0.83	658	–
3.5% NaCl + 5×10^{-5} M HAO (1 h)	10.15	6.45	0.84	1312	49.85
3.5% NaCl + 1×10^{-4} M HAO (1 h)	10.49	5.96	0.86	2034	67.65
3.5% NaCl + 5×10^{-4} M HAO (1 h)	11.31	5.59	0.88	3356	80.39
3.5% NaCl + 0.0 M HAO (48 h)	10.05	7.03	0.85	705	–
3.5% NaCl + 5×10^{-5} M HAO (48 h)	10.62	6.62	0.86	1624	56.59
3.5% NaCl + 1×10^{-4} M HAO (48 h)	10.97	5.17	0.87	2289	69.20
3.5% NaCl + 5×10^{-4} M HAO (48 h)	11.73	4.21	0.89	3835	81.67

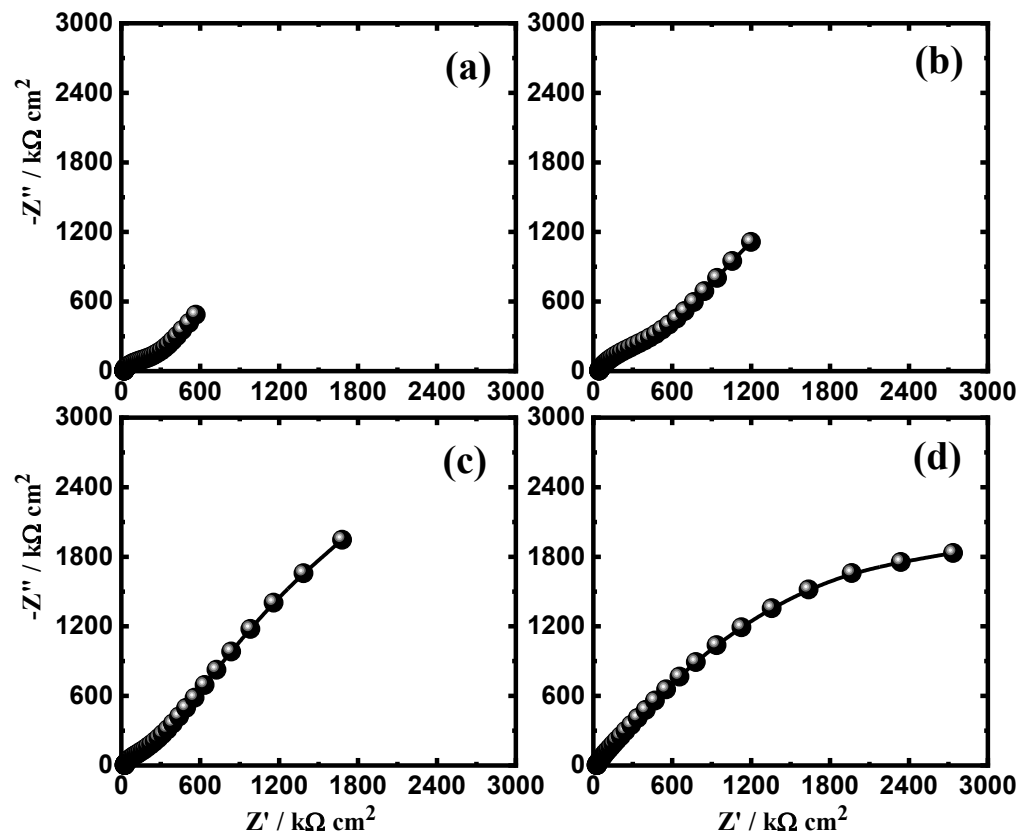


Figure 10. Nyquist plots obtained for iron samples after 1 h immersion in (a) 3.5% NaCl solutions in the absence and presence of (b) 5×10^{-5} M HAO, (c) 1×10^{-4} M HAO, and (d) 5×10^{-4} M HAO.

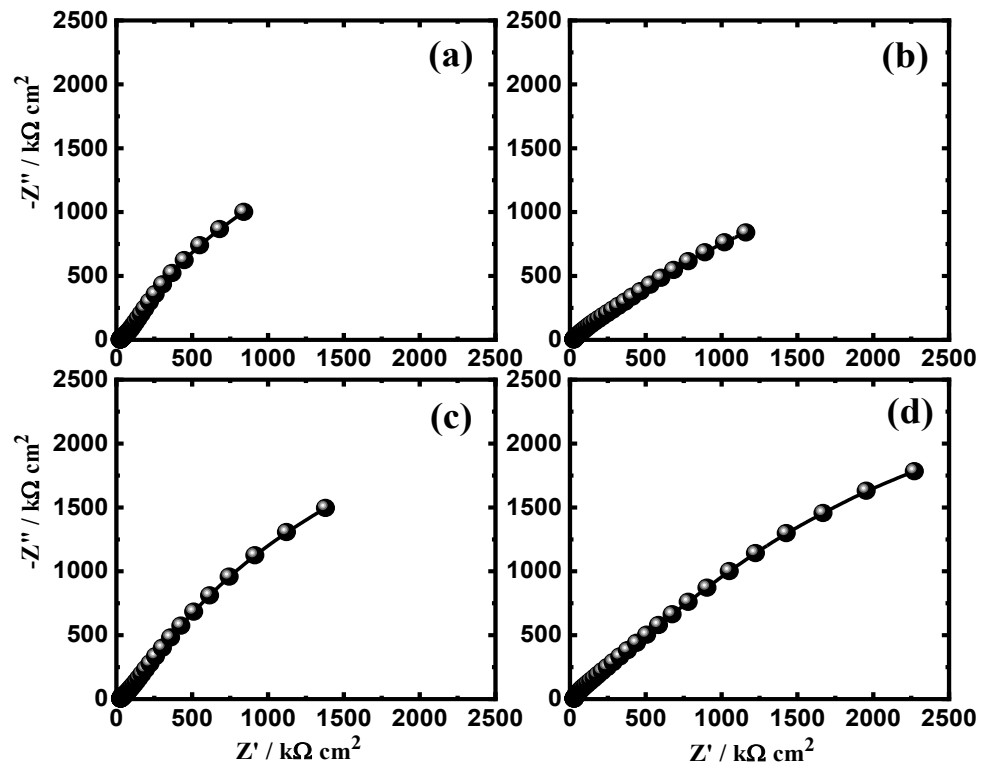


Figure 11. Nyquist plots obtained for iron rod samples after 48 h immersion in (a) 3.5% NaCl solutions in the absence and presence of (b) 5×10^{-5} M HAO, (c) 1×10^{-4} M HAO, and (d) 5×10^{-4} M HAO.

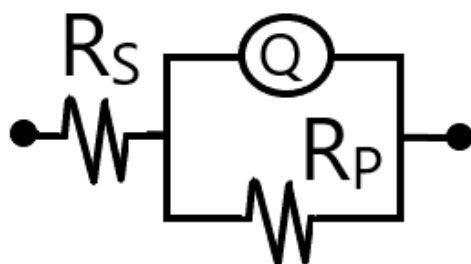


Figure 12. Equivalent circuit model used to fit the EIS experimental data.

Here, R_p^{Un} and R_p^{In} are the values of the polarization resistance without and with HAO, respectively. The Nyquist plots for the iron samples in the different solutions after 1 h as well as after 48 h show only one semicircle, the diameter of which increased in the presence of HAO and with the increase of its concentration. The smallest diameter for the semicircle was obtained for iron after 1 and 48 h immersion in 3.5% NaCl solution in the absence of HAO molecules. Table 3 also shows that the R_S and R_P values were the lowest while the Y_Q were values the highest for iron in chloride solution alone. The presence of the HAO compound increased the corrosion resistance of iron, as indicated by the wide diameter of the Nyquist plot's semicircle. This was confirmed by the R_S and R_P values, which increased with the increase in HAO content within the chloride test solution. The values of Y_Q and the exponent n values varied between 0.83 and 0.89, revealing that Q can be considered as a double layer capacitor with some porosity.

Increasing the immersion period of time from 1 to 48 h before measurement (Figure 11) resulted in almost similar Nyquist plots, whereby the presence of HAO molecules increased the diameter of the drawn semicircle. This effect increased with the increases in HAO from 5×10^{-5} M to 1×10^{-4} M and further to 5×10^{-4} M. Looking at the digits listed in Table 3, the values of R_S , R_P , and $IE\%$ greatly increase with the increase in HAO content and further with the increase in immersion time to 48 h as compared to the shorter exposure period of 1 h. The values of Y_Q also decreased with the content of HAO and with the increase in immersion time. The EIS data, thus, were in good agreement with the data collected via polarization, confirming the fact that the increase in HAO content and extended immersion time increased the corrosion resistance of the iron in the chloride solution.

3.2.4. Scanning Electron Microscopy (SEM) and Energy-Dispersive X-ray (EDX) Analyses

The SEM image and EDX spectra obtained from the surface of iron after its immersion for 48 h in 3.5% NaCl solution (before applying a potential amount of -475 mV (Ag/AgCl) for 60 min) are shown in Figure 13. The SEM micrograph shows numerous pits spreading over the surface of the iron sample. This confirms that the increase in the current with time that is shown in Figure 8 (curve 1) was due to the occurrence of pitting corrosion. The EDX profile analysis indicated that the atomic percentages (at%) for the elements found on the iron samples were 72.54% Fe, 13.53% O, 12.46% C, 0.78% Na, and 0.68% Cl. The at% values for Fe and O were the highest, revealing that the layer formed on the surface during the current–time experiment was mostly iron oxide, as represented by Reactions (6) and (7). The low at% values for both Na and Cl resulted from the deposition of a thin layer of NaCl salt on the surface.

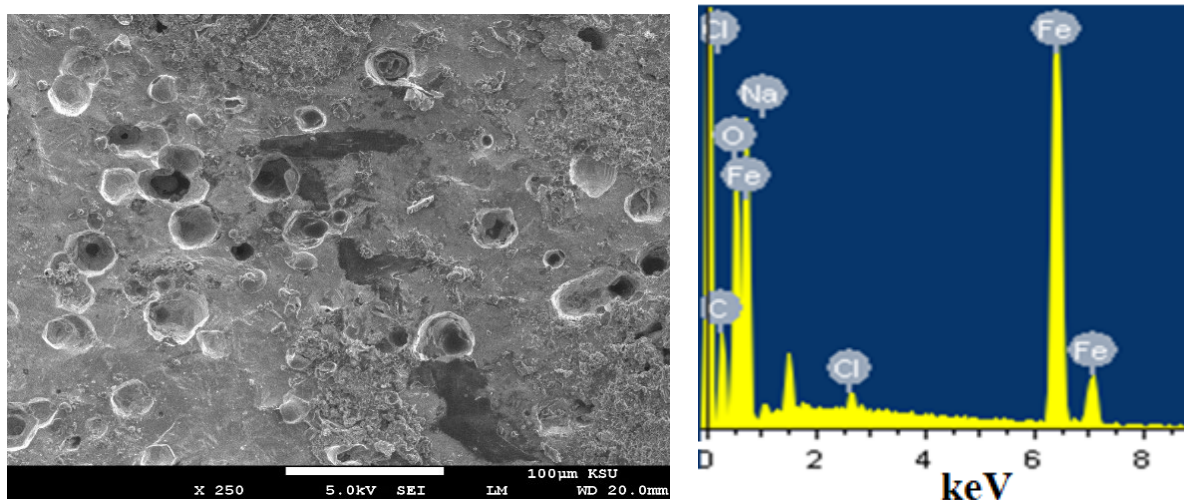


Figure 13. SEM image and EDX profile spectrum after 1 h with a potential of -475 mV (Ag/AgCl) for the surface of the iron rod that was immersed for 48 h in 3.5% NaCl solution before measurement.

Figure 14 shows the SEM micrograph and EDX profile taken from the surface of the iron sample that was left in 3.5% NaCl + 1×10^{-4} M HAO for 48 h before setting the potential to -475 mV (Ag/AgCl) for 1 h. It can be seen from the SEM image that the sample shows no pitting but does show the formation of a surface layer. This layer was most probably due to the surface of iron being in contact with the electrolyte. In order to confirm the composition of the layers formed on the surface, the EDX analysis was carried out. The at% percentages for the majority of the surfaces were 55.88% Fe, 32.48% O, 7.60% C, 2.61% Cl, and 1.43% Na. It is clear that the highest at% values were obtained for Fe and O. As compared to the surface in chloride solution alone, the at% of O was too high but the at% for Fe was too low. This meant that the iron had a thick protective layer that covered its surface and prevented its corrosion thanks to the presence of HAO molecules within the chloride solution. The presence of Cl and Na at these low percentages was due to the adsorption of a thin layer of NaCl salt on the surface of the iron sample. The spectroscopic investigations confirmed the electrochemical measurements showing that the presence of HAO molecules and increases in their concentration increase the corrosion resistance for iron in 3.5% NaCl solution.

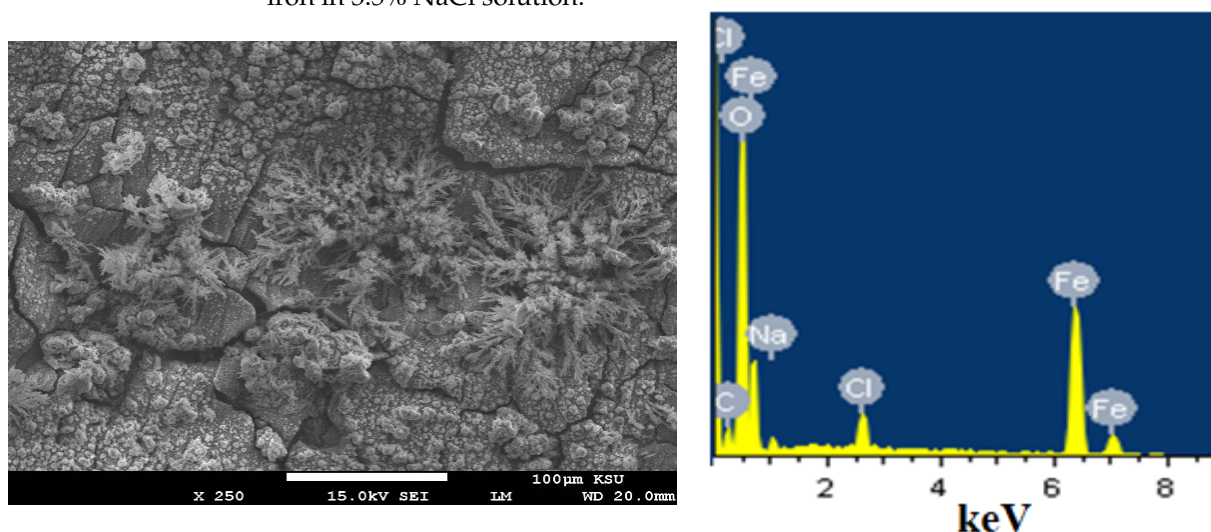
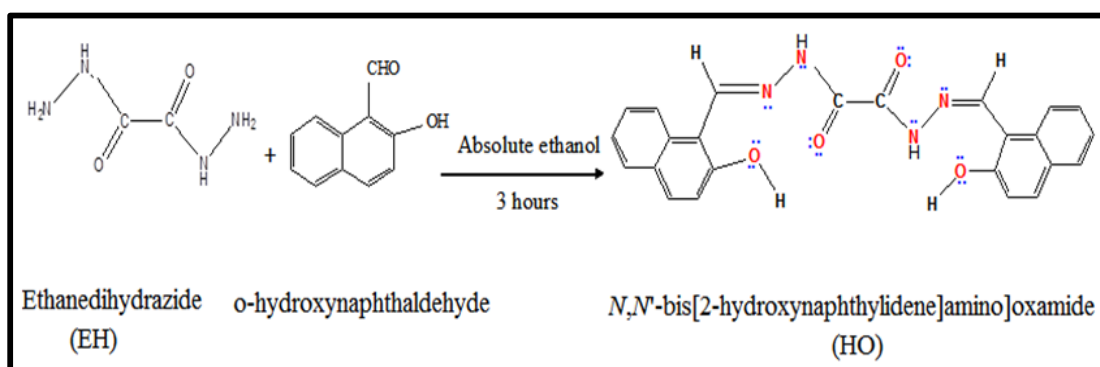


Figure 14. SEM image and EDX profile spectrum after 1 h with a potential of -475 mV (Ag/AgCl) for the surface of an iron sample that was immersed for 48 h in 3.5% NaCl solution containing 1×10^{-4} M HAO before measurement.

The theory of hard and soft acids and bases (HSAB) can also explain the theory of inhibition. According to Ralph G. Pearson's principle [59,60], metals (M) are classified into three classes, namely hard acids, soft acids, and intermediate (borderline) acids. Bases are also classified into hard, soft, and intermediate (borderline) bases. Hard metals, i.e., those with a high charge and small size (charge/size = high), tend to bind with hard bases containing F^- and O donor atoms. Based on this supposition along with the obtained data, it can be concluded that iron ions (Fe^{2+}), which are classified as hard acids, will bind strongly with the inhibitor containing O donor atoms in its structure (Scheme 1). Moreover, the persistence of the N donor in the HAO structure may also help its binding with iron ions, as it is associated with intermediate bases.



Scheme 1. Synthesis and proposed structure of the investigated inhibitor (HAO).

4. Conclusions

The *N,N'*-bis[2-hydroxynaphthylidene]amino]oxamide inhibitor (HAO) can be prepared via the usual condensation reaction between ethanedihydrazide and 2-hydroxynaphthalene-1-carbaldehyde in hydrazide–aldehyde molar ratio of 1:2. Elemental analysis (CHN), UV–Vis spectra, FT-IR spectroscopy, and 1H and ^{13}C NMR spectra showed the identity of the inhibitor. Electrochemical experiments proved that iron corrodes in chloride solution via both uniform and pitting corrosion. Regarding the effects of the time of exposure at 1 and 48 h, it was found that increased time of exposure led to less uniform corrosion. The addition of a low concentration of HAO of 5×10^{-5} M to the chloride solution was found to mitigate the corrosion of iron by decreasing its j_{Corr} and K_{Corr} as well as increasing its R_p . Increasing the content of HAO to 1×10^{-4} M and more to 5×10^{-4} M greatly inhibited the corrosion of iron by decreasing all its corrosion reactions, which was reflected its decreased values of K_{Corr} and increased values of R_p . Furthermore, the extension of the exposure time to 48 h enhanced the effects of HAO in terms of the inhibition of iron corrosion. The results revealed iron suffered uniform and pitting corrosion in NaCl solution and that HAO molecules inhibit this corrosion, particularly at high concentrations and after long immersion periods.

Author Contributions: Conceptualization, E.-S.M.S. and A.H.A.; methodology, E.-S.M.S., A.H.A., H.S.A. and M.N.D.; formal analysis, E.-S.M.S., A.H.A. and M.N.D.; writing—original draft preparation, E.-S.M.S. and A.H.A.; writing—review and editing, E.-S.M.S. and A.H.A.; supervision, E.-S.M.S. and A.H.A.; project administration, E.-S.M.S. and A.H.A. All authors have read and agreed to the published version of the manuscript.

Funding: This work acknowledges the fund from the King Saud University, Deanship of Scientific Research, College of Engineering Research Center.

Institutional Review Board Statement: Not applicable.

Informed Consent Statement: Not applicable.

Data Availability Statement: The data presented in this study are available within the manuscript.

Acknowledgments: The authors would like to extend their sincere appreciation to the King Saud University, Deanship of Scientific Research, College of Engineering Research Center for Funding.

Conflicts of Interest: The authors declare no competing financial interest.

References

1. Rollas, S.; Kucukguzel, S.G. Biological activities of hydrazone derivatives. *Molecules* **2007**, *12*, 1910–1939. [[CrossRef](#)]
2. Barbazan, P.; Carballo, R.; Covelo, B.; Lodeiro, C.; Lima, J.C.; Vazquez-Lopez, E.M. Synthesis, characterization, and photophysical properties of 2-hydroxybenzaldehyde [(1E)-1-pyridin-2-ylethylidene]hydrazone and its rhenium(I) complexes. *Eur. J. Inorg. Chem.* **2008**, *2008*, 2713–2720. [[CrossRef](#)]
3. Berger, S.A.; Ryan, D.E. The use of substituted hydrazones as metallochromic indicators: The EDTA titration of copper. *Mikrochim. Acta* **1974**, *62*, 679–688. [[CrossRef](#)]
4. Odashima, T.; Anzai, F.; Ishii, H. Substituted 2-thiophenealdehyde-2-benzothiazolyl-hydrazones as analytical reagents for copper. *Anal. Chim. Acta* **1976**, *86*, 231–236. [[CrossRef](#)]
5. Berger, S.A. The Liquid-Liquid Extraction of Copper(II), Nickel(II), and Cobalt(II) with 2,2'-Pyridil-mono-(2-quinoly)hydrazone). *Microchem. J.* **1993**, *47*, 317–324. [[CrossRef](#)]
6. Berger, S.A. Benzil-mono-(2-quinoly)-hydrazone as a chelating agent for copper. *Mikrochim. Acta* **1979**, *71*, 311–316. [[CrossRef](#)]
7. Macedo, M.C.S.S.; Barcia, O.E.; Da Silva, E.C.; Mendes, J.D. Corrosion inhibition of iron in NaCl 3.5% by some derivatives imidazole. *J. Electrochem. Soc.* **2012**, *159*, C160. [[CrossRef](#)]
8. Aslam, R.; Mobin, M.; Aslam, J.; Lgaz, H. Sugar based *N,N'*didodecyl-*N,N'*digluconamideethylenediamine gemini surfactant as corrosion inhibitor for mild steel in 3.5% NaCl solution-effect of synergistic KI additive. *Sci. Rep.* **2018**, *8*, 3690. [[CrossRef](#)] [[PubMed](#)]
9. Sherif, E.-S.M. Corrosion and corrosion inhibition of pure iron in neutral chloride solutions by 1,1'-thiocarbonyldiimidazole. *Int. J. Electrochem. Sci.* **2011**, *6*, 3077–3092.
10. Sherif, E.-S.M. Effects of 5-(3-aminophenyl)-tetrazole on the inhibition of unalloyed iron corrosion in aerated 3.5% sodium chloride solutions as a corrosion inhibitor. *Mater. Chem. Phys.* **2011**, *129*, 961–967. [[CrossRef](#)]
11. Zhu, H.; Li, X.; Lu, X.; Chen, X.; Li, J.; Han, X.; Ma, X.; Hu, Z. Intra-/inter-molecular synergistic inhibition effect of sulfonate surfactant and 2-benzothiazolethiol on carbon steel corrosion in 3.5% NaCl solution. *Corros. Sci.* **2021**, *182*, 109291. [[CrossRef](#)]
12. Sherif, E.-S.M. Corrosion inhibition in chloride solutions of iron by 3-amino-1,2,4-triazole-5-thiol and 1,1'-thiocarbonyldiimidazole. *Int. J. Electrochem. Sci.* **2012**, *7*, 4834–4846.
13. Zhang, Z.; Wang, F.; Liu, Y.; Wu, S.; Li, W.; Sun, W.; Guod, D.; Jiang, J. Molecule adsorption and corrosion mechanism of steel under protection of inhibitor in a simulated concrete solution with 3.5% NaCl. *RSC Adv.* **2018**, *8*, 20648. [[CrossRef](#)]
14. Velrani, S.; Jeyaprabha, B.; Prakash, P. Inhibition of mild steel corrosion in 3.5% NaCl medium using 1-butyl-3-methylimidazolium chloride. *Int. J. Innov. Sci. Eng. Technol.* **2014**, *1*, 57–69.
15. Shahzad, K.; Sliem, M.H.; Shakoob, R.A.; Radwan, A.B.; Kahraman, R.; Umer, M.A.; Manzoor, U.; Abdullah, A.M. Electrochemical and thermodynamic study on the corrosion performance of API X120 steel in 3.5% NaCl solution. *Sci. Rep.* **2020**, *10*, 4314. [[CrossRef](#)]
16. ArockiaSelvi, J.; Kamaraj, P.; Arthanareeswari, M.; PushpaMalini, T.; Mohanapriya, S.; Subasree, N. Effect of cetylpyridinium chloride on corrosion inhibition of mild steel in chloride environment. *Mater. Today* **2019**, *14*, 264–270. [[CrossRef](#)]
17. Sherif, E.-S.M.; Ahmed, A.H. Synthesizing new hydrazone derivatives and studying their effects on the inhibition of copper corrosion in sodium chloride solutions. *Synth. React. Inorg. Met.-Org. Nano-Met. Chem.* **2010**, *40*, 365–372. [[CrossRef](#)]
18. Mohammad, O.; Khamaysa, A.; Selatnia, I.; Zeghache, H.; Lgaz, H.; Benahmed, M.; Gherraf, N.; Mosset, P. Enhanced corrosion inhibition of carbon steel in HCl solution by a newly synthesized hydrazine derivative: Mechanism exploration from electrochemical, XPS, and computational studies. *J. Mol. Liq.* **2020**, *315*, 113805.
19. Lgaz, H.; Salghi, R.; Masroor, S.; Kim, S.; Kwon, C.; Kim, S.Y.; Yang, Y.; Chung, I.-M. Assessing corrosion inhibition characteristics of hydrazone derivatives on mild steel in HCl: Insights from electronic-scale DFT and atomic-scale molecular dynamics. *J. Mol. Liq.* **2020**, *308*, 112998. [[CrossRef](#)]
20. Lgaz, H.; Chung, I.-M.; Albayati, M.R.; Chaouiki, A.; Salghi, R.; Mohamed, S.K. Improved corrosion resistance of mild steel in acidic solution by hydrazone derivatives: An experimental and computational study. *Arab. J. Chem.* **2020**, *13*, 2934–2954. [[CrossRef](#)]
21. Chafai, N.; Chafaa, S.; Benbouguerra, K.; Hellala, A.; Mehri, M. Synthesis, spectral analysis, anti-corrosive activity and theoretical study of an aromatic hydrazone derivative. *J. Mol. Struct.* **2019**, *1181*, 83–92. [[CrossRef](#)]
22. Chaouiki, A.; Chafiq, M.; Lgaz, H.; Al-Hadeethi, M.R.; Ali, I.; Masroor, S.; Chung, I.-M. Green corrosion inhibition of mild steel by hydrazone derivatives in 1.0 M HCl. *Coatings* **2020**, *10*, 640. [[CrossRef](#)]
23. Fouda, A.S.; Badr, G.E.; El-Haddad, M.N. The inhibition of c-steel corrosion in H₃PO₄ solution by some furfural hydrazone derivatives. *J. Korean Chem. Soc.* **2008**, *52*, 124–132. [[CrossRef](#)]
24. Gnanasekaran, M.; Mohan, K.; Kumaravel, A.; Magibalan, S. Characterization, corrosion behavior, effect of temperature and inhibition studies on AA6351 frictional surfaced mild steel. *J. Mater. Res. Technol.* **2020**, *9*, 16080–16092. [[CrossRef](#)]

25. Ahmed, A.H.; Hassan, A.M.; Gumaa, H.A.; Mohamed, B.H.; Eraky, A.M.; Omran, A.A. Copper(II)-oxaloyldihydrazone complexes: Physico-chemical studies; energy band gap and inhibition evaluation of free oxaloyldihydrazones toward the corrosion of copper metal in acidic medium. *Arab. J. Chem.* **2019**, *12*, 4287–4302. [[CrossRef](#)]
26. Ahmed, A.H.; Hassan, A.M.; Gumaa, H.A.; Mohamed, B.H.; Eraky, A.M. Physicochemical studies on some selected oxaloyldihydrazones and their novel palladium(II) complexes along with using oxaloyldihydrazones as corrosion resistants. *Inorg. Nano-Met. Chem.* **2017**, *47*, 1652–1663. [[CrossRef](#)]
27. Ahmed, A.H.; Hassan, A.M.; Gumaa, H.A.; Mohamed, B.H.; Eraky, A.M. Mn²⁺-complexes of N,O-dihydrazone: Structural studies, indirect band gap energy and corrosion inhibition on aluminum in acidic medium. *J. Chil. Chem. Soc.* **2018**, *63*, 4159–4168. [[CrossRef](#)]
28. Chetouani, A.; Aouniti, A.; Hammouti, B.; Benchat, N.; Benhadda, T.; Kertit, S. Corrosion inhibitors for iron in hydrochloride acid solution by newly synthesised pyridazine derivatives. *Corros. Sci.* **2003**, *45*, 1675–16784. [[CrossRef](#)]
29. Zhao, P.; Liang, Q.; Li, Y. Electrochemical, SEM/EDS and quantum chemical study of phthalocyanines as corrosion inhibitors for mild steel in 1 mol/L HCl. *J. Appl. Surf. Sci.* **2005**, *252*, 1596–1607. [[CrossRef](#)]
30. Sherif, E.-S.M. Effects of 2-amino-5-(ethylthio)-1,3,4-thiadiazole on copper corrosion as a corrosion inhibitor in 3% NaCl solutions. *J. Appl. Surf. Sci.* **2006**, *252*, 8615–8622. [[CrossRef](#)]
31. Yao, J.L.; Ren, B.; Huang, Z.F.; Cao, P.G.; Gub, R.A.; Tian, Z.-Q. Extending surface raman spectroscopy to transition metals for practical applications IV. A study on corrosion inhibition of benzotriazole on bare Fe electrodes. *Electrochim. Acta* **2003**, *48*, 1263–1271. [[CrossRef](#)]
32. Bazzaoui, M.; Martins, L.; Bazzaoui, E.A.; Martins, J.I. New single-step electrosynthesis process of homogeneous and strongly adherent polypyrrole films on iron electrodes in aqueous medium. *Electrochim. Acta* **2002**, *47*, 2953–2962. [[CrossRef](#)]
33. Zawada, K.; Bukowska, J.; Calvo, M.; Jackowska, K. Surface-enhanced raman spectroscopy and electrochemistry at the copper | 4-phenylpyridine interface. *Electrochim. Acta* **2001**, *46*, 2671–2680. [[CrossRef](#)]
34. Sherif, E.M.; Park, S.-M. Effects of 1,5-Naphthalenediol on aluminum corrosion as a corrosion inhibitor in 0.50 M NaCl. *J. Electrochem. Soc.* **2005**, *152*, B205–B211. [[CrossRef](#)]
35. Sherif, E.M.; Park, S.-M. Effects of 1,4-naphthoquinone on aluminum corrosion in 0.50 M sodium chloride solutions. *Electrochim. Acta* **2006**, *51*, 1313–1321. [[CrossRef](#)]
36. Ahmed, A.H.; Sherif, E.-S.M.; Abdo, H.S.; Gad, E.S. Ethanedihydrazone as a corrosion inhibitor for Iron in 3.5% NaCl solutions. *ACS Omega* **2021**, *6*, 14525–14532. [[CrossRef](#)]
37. Abdallah, M. Rhodanine azosulpha drugs as corrosion inhibitors for corrosion of 304 stainless steel in hydrochloric acid solution. *Corros. Sci.* **2002**, *44*, 717–728. [[CrossRef](#)]
38. Abd El Maksoud, S.A. Studies on the effect of pyranocoumarin derivatives on the corrosion of iron in 0.5 M HCl. *Corros. Sci.* **2002**, *44*, 803–813. [[CrossRef](#)]
39. Quraishi, M.A.; Rawat, J. Inhibition of mild steel corrosion by some macrocyclic compounds in hot and concentrated hydrochloric acid. *Mater. Chem. Phys.* **2002**, *73*, 118–122. [[CrossRef](#)]
40. Salama, T.M.; Ahmed, A.H.; El-Bahy, Z.M. Y-type zeolite-encapsulated copper (II) salicylidene-p-aminobenzoic Schiff base complex: Synthesis, characterization and carbon monoxide adsorption. *Micropor. Mesopor. Mater.* **2006**, *89*, 251–259. [[CrossRef](#)]
41. Ahmed, A.H. N,N'-bis[2-hydroxynaphthylidene]/[2-methoxybenzylidene]amino]oxamides and their divalent manganese complexes: Isolation, spectral characterization, morphology, antibacterial and cytotoxicity against leukemia cells. *Open Chem.* **2020**, *18*, 426–437. [[CrossRef](#)]
42. Ahmed, A.H.; Hassan, A.M.; Gumaa, H.A.; Mohamed, B.H.; Eraky, A.M. Nickel(II)-oxaloyldihydrazone complexes: Characterization, indirect band gap energy and antimicrobial evaluation. *Cogent Chem.* **2016**, *2*, 1142820. [[CrossRef](#)]
43. Ahmed, A.H.; Moustafa, M.G. Spectroscopic, morphology and electrical conductivity studies on Co(II), Ni(II), Cu(II) and Mn(II)-oxaloyldihydrazone complexes. *J. Saudi Chem. Soc.* **2020**, *24*, 381–392. [[CrossRef](#)]
44. Sherif, E.-S.M.; Erasmus, R.M.; Comins, J.D. In situ Raman spectroscopy and electrochemical techniques for studying corrosion and corrosion inhibition of iron in sodium chloride solutions. *Electrochim. Acta* **2010**, *55*, 3657–3663. [[CrossRef](#)]
45. Sherif, E.-S.M.; Erasmus, R.M.; Comins, J.D. Corrosion of copper in aerated synthetic sea water solutions and its inhibition by 3-amino-1,2,4-triazole. *J. Colloid Interface Sci.* **2007**, *309*, 470–477. [[CrossRef](#)]
46. Zhang, Z.; Chen, S.; Li, Y.; Li, S.; Wang, L. A study of the inhibition of iron corrosion by imidazole and its derivatives self-assembled films. *Corros. Sci.* **2009**, *51*, 291–300. [[CrossRef](#)]
47. Sherif, E.-S.M.; Almajid, A.A. Corrosion of magnesium/manganese alloy in chloride solutions and its inhibition by 5-(3-aminophenyl)-tetrazole. *Int. J. Electrochem. Sci.* **2011**, *6*, 2131–2148.
48. Sherif, E.M.; Park, S.-M. 2-Amino-5-ethyl-1,3,4-thiadiazole as a corrosion inhibitor for copper in 3.0% NaCl solutions. *Corros. Sci.* **2006**, *48*, 4065–4079. [[CrossRef](#)]
49. Khalil, K.A.; Sherif, E.-S.M.; Almajid, A.A. Corrosion passivation in simulated body fluid of magnesium/hydroxyapatite nanocomposites sintered by high frequency induction heating. *Int. J. Electrochem. Sci.* **2011**, *6*, 6184–6199.
50. Sherif, E.-S.M.; Potgieter, J.H.; Comins, J.D.; Cornish, L.; Olubambi, P.A.; Machio, C.N. The beneficial effect of ruthenium additions on the passivation of duplex stainless steel corrosion in sodium chloride solutions. *Corros. Sci.* **2009**, *51*, 1364–1371. [[CrossRef](#)]
51. Sherif, E.-S.M.; Latief, F.H.; Abdo, H.S.; Alharthi, N.H. Electrochemical and spectroscopic study on the corrosion of Ti–5Al and Ti–5Al–5Cu in chloride solutions. *Met. Mater. Int.* **2019**, *25*, 1511–1520. [[CrossRef](#)]

52. Sherif, E.-S.M.; Potgieter, J.H.; Comins, J.D.; Cornish, L.; Olubambi, P.A.; Machio, C.N. Effects of minor additions of ruthenium on the passivation of duplex stainless-steel corrosion in concentrated hydrochloric acid solutions. *J. Appl. Electrochem.* **2009**, *39*, 1385–1392. [[CrossRef](#)]
53. Amin, M.A.; Abd El-Rehim, S.S.; El-Sherbini, E.E.; Bayoumi, R.S. The inhibition of low carbon steel corrosion in hydrochloric acid solutions by succinic acid part I. weight loss, polarization, EIS, PZC, EDX and ESM studies. *Electrochim. Acta* **2007**, *52*, 3588–3599. [[CrossRef](#)]
54. Feliu, S., Jr. Electrochemical impedance spectroscopy for the measurement of the corrosion rate of magnesium alloys: Brief review and challenges. *Metals* **2020**, *10*, 775. [[CrossRef](#)]
55. Kuriakose, N.; Kakkassery, J.T.; Raphael, V.P.; Shanmughan, S.K. Electrochemical impedance spectroscopy and potentiodynamic polarization analysis on anticorrosive activity of thiophene-2-carbaldehyde derivative in acid medium. *Ind. J. Mater. Sci.* **2014**, *2014*, 124065. [[CrossRef](#)]
56. Sherif, E.M.; Park, S.-M. Effects of 2-amino-5-ethylthio-1,3,4-thiadiazole on copper corrosion as a corrosion inhibitor in aerated acidic pickling solutions. *Electrochim. Acta* **2006**, *51*, 6556–6562. [[CrossRef](#)]
57. Sherif, E.M.; Park, S.-M. Inhibition of copper corrosion in acidic pickling solutions by N-phenyl-1,4-phenylenediamine. *Electrochim. Acta* **2006**, *51*, 4665–4673. [[CrossRef](#)]
58. Sherif, E.M.; Park, S.-M. Inhibition of copper corrosion in 3.0% NaCl by N-phenyl-1,4-phenylenediamine. *J. Electrochem. Soc.* **2005**, *152*, 428–433. [[CrossRef](#)]
59. Pearson, R.G. Hard and soft acids and bases, HSAB, part II: Underlying theories. *J. Chem. Educ.* **1968**, *45*, 643–648. [[CrossRef](#)]
60. Pearson, R.G. *Chemical Hardness—Applications from Molecules to Solids*; Wiley-VCH: Weinheim, Germany, 1997.